

Simulation of extreme rainfall and projection of future changes using the GLIMCLIM model

Md. Mamunur Rashid^{1,2} · Simon Beecham¹ · Rezaul Kabir Chowdhury^{1,3}

Received: 5 January 2015 / Accepted: 10 August 2016 / Published online: 20 August 2016
© Springer-Verlag Wien 2016

Abstract In this study, the performance of the Generalized Linear Modelling of daily CLimate sequence (GLIMCLIM) statistical downscaling model was assessed to simulate extreme rainfall indices and annual maximum daily rainfall (AMDR) when downscaled daily rainfall from National Centers for Environmental Prediction (NCEP) reanalysis and Coupled Model Intercomparison Project Phase 5 (CMIP5) general circulation models (GCM) (four GCMs and two scenarios) output datasets and then their changes were estimated for the future period 2041–2060. The model was able to reproduce the monthly variations in the extreme rainfall indices reasonably well when forced by the NCEP reanalysis datasets. Frequency Adapted Quantile Mapping (FAQM) was used to remove bias in the simulated daily rainfall when forced by CMIP5 GCMs, which reduced the discrepancy between observed and simulated extreme rainfall indices. Although the observed AMDR were within the 2.5th and 97.5th percentiles of the simulated AMDR, the model consistently under-predicted the inter-annual variability of AMDR. A non-stationary model was developed using the generalized linear model for local, shape and scale to estimate the AMDR with an annual exceedance probability of 0.01. The study shows

that in general, AMDR is likely to decrease in the future. The Onkaparinga catchment will also experience drier conditions due to an increase in consecutive dry days coinciding with decreases in heavy (>long term 90th percentile) rainfall days, empirical 90th quantile of rainfall and maximum 5-day consecutive total rainfall for the future period (2041–2060) compared to the base period (1961–2000).

1 Introduction

An increase in greenhouse gas emissions is raising the earth's average temperatures and resulting in climate change around the world. This has changed the frequency, magnitude and persistence of extreme events of various climatic variables, including rainfall, which has been identified in observational records (Alexander et al. 2006; Alexander and Arblaster 2009; Evans et al. 2009; Frich et al. 2002). According to the Intergovernmental Panel on Climate Change (IPCC) Fourth Assessment Report (AR4, IPCC 2007), climate change has started to affect the frequency, intensity and duration of extreme temperature, rainfall and drought almost everywhere around the world over the late twentieth century and this will continue in future. This is also confirmed by the recent assessment by IPCC in the special report on Managing the Risks of Extreme Events and Disasters to Advance Climate Change Adaptation (SREX, IPCC 2012). Projections of future changes in climate extremes are of particular interest due to their adverse effects on society and ecosystems.

Significant changes in extreme temperature and rainfall during the twentieth century across Australia have already been identified in previous studies (Alexander et al. 2006; Alexander and Arblaster 2009; Alexander et al. 2007; Collins et al. 2000; Evans et al. 2009; Hennessy et al. 1999; Plummer et al. 1999; Suppiah and Hennessy 1998). Over the last century, a significant

✉ Md. Mamunur Rashid
mdmamunur.rashid@mymail.unisa.edu.au;
md.rashid@unsw.edu.au

¹ Natural and Built Environments Research Centre, School of Natural and Built Environments, University of South Australia, Mawson Lakes, SA 5095, Australia

² Water Research Centre, University of New South Wales, Sydney, NSW 2052, Australia

³ Department of Civil and Environmental Engineering, United Arab Emirates University, Al Ain 15551, United Arab Emirates

decrease in the frequency and intensity of extreme rainfall events was observed in the southwest region of Western Australia. It has also been reported that there has been a significant increase in the proportion of total rainfall from extreme events in eastern Australia (Haylock and Nicholls 2000; Li et al. 2005). Alexander and Arblaster (2009) observed that Australia is likely to shift toward increased temperature extremes and much longer dry spells with increased extreme rainfall according to the Coupled Model Intercomparison Project Phase 5 (CMIP5) general circulation models (GCMs). Sillmann et al. (2013) concluded that according to CMIP5 GCM results, Australia will experience dry conditions due to an increase in consecutive dry days coinciding with a decrease in both heavy precipitation days and maximum consecutive 5-day precipitation over the twenty-first century relative to their base period of 1981–2000.

Extreme climate events in South Australia (SA), particularly droughts, cause severe economic losses for the state's agricultural industries and rural populations. In this regard, the future projection of extreme events is important for climate change adaptation purposes. However, to date, there has been very limited research that has attempted to assess the future changes in extreme climate at the regional level in SA using CMIP5 GCMs which include more sophisticated climate models and a new suite of forcing scenarios compared to the former CMIP3 models. In CMIP5, approximately half of the GCMs have an average longitudinal resolution finer than 1.3° whereas in CMIP3 only one model fell into this category (Teng et al. 2012). The CMIP5 models have been found to be more skilful than CMIP3 models in reproducing the Asian-Australian monsoon (AAM) (Wang et al. 2014). Sillmann et al. (2013) concluded that CMIP5 ensembles provide some improvement to CMIP3 ones in the representation of the magnitude of extreme precipitation indices, and this improvement is partly due to the higher spatial resolution of CMIP5 models compared to CMIP3 models. In a recent study, Rashid et al. (2015) observed that the 95th percentile of daily rainfall is likely to decrease over the period 2041–2060 compared to the historical period of 1961–2000 using statistically down-scaled daily rainfall from CMIP5 GCM outputs.

GCMs are a widely used tool to project future climate change under different greenhouse gas emission scenarios (Chu et al. 2010; Hu et al. 2012; Huang et al. 2011; King et al. 2012; Sachindra et al. 2014). Due to the coarse resolution of GCM outputs, they are limited in their ability to capture meteorological processes at sufficiently fine resolutions, and consequently, they generally cannot be directly used for local-scale projections. In order to resolve this issue, GCM output datasets are often down-scaled to a finer resolution for climate change impact studies. Downscaling methods are broadly divided into two classes, namely dynamic and statistical. Statistical downscaling is more widely used due to its ease of application and reduced cost. The Generalized Linear Modelling of daily CLimate sequence (GLIMCLIM) is a multi-site stochastic downscaling model based on a generalized linear model (GLM) (Chandler 2002),

which has been used around the world (Beecham et al. 2014; Frost et al. 2011; Kigobe et al. 2011; Liu et al. 2012; Mehrotra et al. 2009; Mirshahi et al. 2008). Although application of GLMs for multi-site stochastic rainfall simulation is relatively new, successful application of this model in Australia is available in recent studies (Beecham et al. 2014; Frost 2007; Frost et al. 2011). Rashid et al. (2015) and Beecham et al. (2014) found that GLIMCLIM was able to downscale historical and projected daily rainfall from the National Centers for Environmental Prediction/National Center for Atmospheric Research (NCEP/NCAR) re-analysis (termed as NCEP reanalysis hereafter) data and CMIP5 GCM outputs in the Onkaparinga catchment in SA. While the GLIMCLIM model has been successfully applied for downscaling of daily rainfall, few studies have assessed its capability to reproduce extreme rainfall. Previous studies have identified that the GLIMCLIM model performed better than other downscaling models including the non-homogeneous hidden Markov model (NHMM) and the statistical downscaling model (SDSM) in reproducing the temporal dependence related extreme rainfall indices such as annual wet/dry days and wet/dry spell lengths (Hu et al. 2013; Liu et al. 2012).

Two types of descriptions are generally used to analyse rainfall extremes (Klein Tank et al. 2009). One is based on the various climate extreme indices that represent moderate meteorological extremes with re-occurrence periods of year, seasonal or monthly (Alexander et al. 2006; Huang et al. 2012; Hundecha and Bárdossy 2008; Jeong et al. 2012; Tebaldi et al. 2006; Yang et al. 2011). The other approach involves fitting a distribution to the annual extreme rainfall and then to estimate the extreme events with multi-year to multi-decadal recurrence commonly known as frequency analysis of annual maximum daily rainfall (Frei et al. 2006; Hashmi et al. 2011; Kharin et al. 2007; Tryhorn and DeGaetano 2011). This approach is important for engineering design and planning.

The classical frequency analysis technique considering the stationary condition is no longer valid in the context of climate change (López and Francés 2013; Trambly et al. 2013; Villarini et al. 2009). One way of incorporating non-stationarity in the frequency model might be by making the distribution parameters dependent on large-scale climatic variables such as NCEP reanalysis and/or GCM output datasets. To date, only a few research studies have considered climatic variables rather than time as covariates in a non-stationary frequency model. Over the last decade, some researchers have successfully incorporated climatic variables as external covariates for non-stationary frequency analysis (Aissaoui-Fqayeh et al. 2009; El Adlouni et al. 2007; Kwon et al. 2008; López and Francés 2013; Ouarda and El-Adlouni 2011; Trambly et al. 2013). The generalized additive model for location, scale and shape (GAMLSS), proposed by Rigby and Stasinopoulos (2005), provides a flexible modelling framework. The dependence of the distribution parameters on the covariates can be represented in terms of linear or non-linear, parametric and/or

additive non-parametric functions. GAMLSS has been successfully used by López and Francés (2013) and Villarini et al. (2009) for non-stationary frequency analysis.

The objectives of the research described in this paper are to assess the performance of the GLIMCLIM downscaling model in terms of simulating extreme rainfall using downscaled daily rainfall from NCEP reanalysis and CMIP5 GCM outputs and to estimate changes for the future period 2041–2060 compared to the base period of 1961–2000. In doing so, Frequency Adapted Quantile Mapping (FAQM) was applied to correct the bias in the simulated daily rainfall and a non-stationary frequency analysis was employed to estimate the annual maximum daily rainfall (AMDR) for an exceedance probability of 0.01 (equivalent to a 100-year annual recurrence interval for stationary frequency analysis). This will be termed as the 100-year AMDR hereafter.

2 Study area and data

The study focuses on the Onkaparinga catchment in SA. The catchment is situated approximately 25 km to the southeast of the city of Adelaide. Being a significant source of water supply for metropolitan Adelaide as well as providing water to farm dams and for the natural environment to maintain environmental flows, the water resources of the Onkaparinga catchment are crucial. Moreover, strong spatial variability of rainfall over this small catchment of approximately 560 km² in area makes it a challenging case study catchment for modelling and downscaling of extreme rainfall (Rashid et al. 2014). Heneker and Cresswell (2010) studied climate change impacts in the Mount Lofty Ranges (MLR) and estimated that there would be a 30 % potential reduction in the annual runoff in the Onkaparinga catchment over the period 2035 to 2065. In addition, Teoh (2003) identified that farm dams divert between 8 and 10 % (4.5 GL) of the catchment's surface water and that this was forecast to increase to around 7 to 10 GL under the current management policies, as at 2002. In general, approximately 60 % of water for Adelaide is collected from the catchment, with the remaining demand being met by pumping water from the Murray River. Considering this, a key management issue for the Onkaparinga catchment is the potential risk of climate change to Adelaide's water supply. In order to understand the future changes of extreme rainfall in the catchment, nine rainfall stations were considered as shown in Fig. 1. Details of these rainfall stations are shown in Table 1. These daily rainfall data for the period 1961–2000 were collected from the SILO database of the Queensland Climate Change Centre of Excellence (www.longpaddock.qld.gov.au/silo/).

NCEP reanalysis datasets were collected from the National Oceanic and Atmospheric Administration/Earth System Research Laboratory (NOAA/ESRL) for the period 1961–2000. The model was calibrated and validated using the daily

NCEP reanalysis datasets over the periods 1961–1986 and 1987–2000 respectively. Historical daily outputs of CMIP5 GCMs for the period 1961–2000 and future daily outputs for the period 2041–2060 under Representative Concentration Pathway (RCP) 4.5 and RCP 8.5 scenarios were collected from the Earth System Grid data distribution portal (www.earthsystemgrid.org). NCEP reanalysis and GCM output data were extracted from 12 grid points around the Onkaparinga catchment, as shown in Fig. 1. The GCM outputs were linearly interpolated to match with the NCEP reanalysis resolution (2.5° × 2.5°). Four CMIP5 GCMs were considered in this study, namely CSIRO-MK3.6.0 by the Commonwealth Scientific and Industrial Research Organization in collaboration with the Queensland Climate Change Centre of Excellence (termed CSIRO hereafter), GFDL-ESM2M by NOAA Geophysical Fluid Dynamics Laboratory (termed GFDL hereafter), MIROC-ESM by the Japan Agency for Marine-Earth Science and Technology (termed MIROC hereafter), BCC-CSM 1.1 by the Beijing Climate Center and China Meteorological Administration (termed BCC hereafter) and CanESM2 by the Canadian Centre for Climate Modelling and Analysis (termed CAN hereafter).

3 Methodology

3.1 Statistical downscaling model

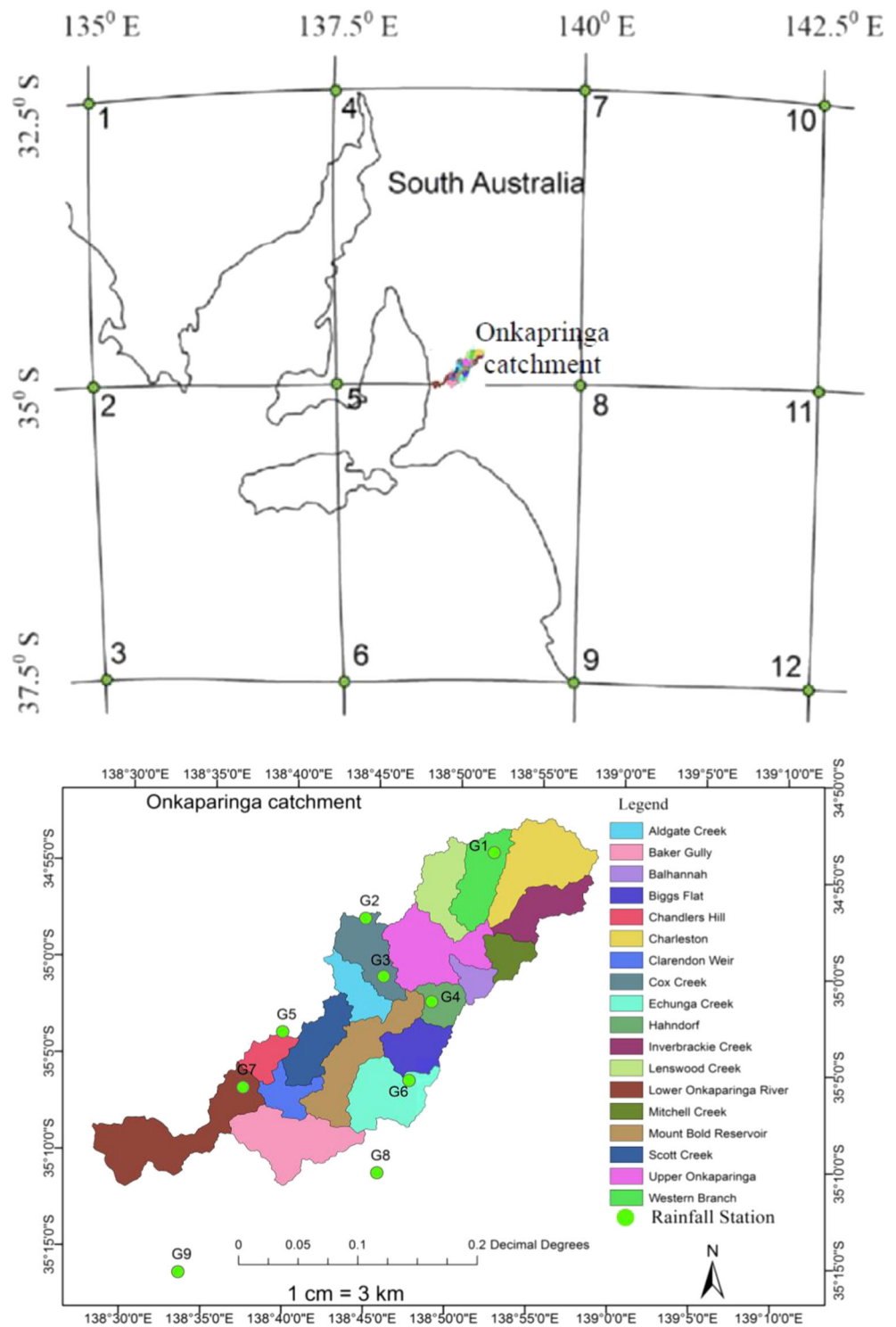
In this study, daily rainfall was statistically downscaled at nine rainfall stations in the Onkaparinga catchment using the GLIMCLIM downscaling model. Details of this model are available in Chandler (2002), Chandler and Wheeler (2002) and Yang et al. (2005). The version of the model used in this study is available at http://www.ucl.ac.uk/~ucajarc/work/software/rain_glm.zip. The application of this model for statistical downscaling of multi-site daily rainfall in SA is reported in Beecham et al. (2014). In GLIMCLIM, the GLM is used to downscale daily rainfall in a two-stage approach. Rainfall occurrence is modelled using logistic regression and then a gamma distribution is used to model the rainfall amount for any wet days. The logistic regression model can be defined as follows (Chandler and Wheeler 2002; Yang et al. 2005):

$$\ln\left(\frac{p_i}{1-p_i}\right) = X_i\beta \quad (1)$$

where p_i is the probability of rain for any day i associated with predictor vector X_i with coefficient vector β . The mean rainfall μ_i for the i th wet day is conditional on a covariate vector ξ_i and coefficient vector α that can be estimated as follows:

$$\ln(\mu_i) = \xi_i\alpha \quad (2)$$

Fig. 1 NCEP reanalysis grid point ($2.5^\circ \times 2.5^\circ$) around the catchment (*top*). Location of the rainfall stations (*bottom*)



Calibration and validation of the model were performed using predictor variables from NCEP reanalysis datasets. The model was calibrated for the period 1961–1986 and validated over the period 1987–2000. Nineteen large-scale atmospheric and circulation variables from NCEP reanalysis datasets were selected as probable predictor variables based on the previous literature which were subsequently reduced to

ten potential variables based on their correlation with observed rainfall. Each predictor variable was extracted from the 12 reanalysis grid points ($2.5^\circ \times 2.5^\circ$) around the study area, and the average of these 12 values gave a single series for each predictor variable used in the downscaling model. Details of the predictor selection process are reported in Beecham et al. (2014). The final selected predictor variables

Table 1 Details of rainfall stations

BOM station ID	Station code	Latitude (decimal degree)	Longitude (decimal degree)	Elevation (m)	Annual median rainfall
023726	G1	-34.9	138.87	459	887
023750	G2	-34.96	138.74	487	1034
023707	G3	-35.01	138.76	445	987
023720	G4	-35.03	138.81	341	779
023709	G5	-35.06	138.66	376	897
023713	G6	-35.1	138.79	370	746
023710	G7	-35.11	138.62	267	756
023730	G8	-35.18	138.76	356	821
023753	G9	-35.27	138.56	104	615

were air temperature at 700 hPa; geopotential height at 700 and 800 hPa; relative humidity at 500, 700 and 850 hPa; zonal wind component at 700 and 850 hPa and meridional wind component at 500 and 700 hPa. The historical (1961–2000) and future (2041–2060) model outputs of four GCMs (CSIRO, GFDL, BCC and CAN) corresponding to the potential predictors were standardized with the means and standard deviations of the NCEP reanalysis outputs of the calibration period. These historical and future model outputs of each GCM were then used in the downscaling model to simulate the past historical rainfall and to project the future rainfall respectively at each of the nine stations in the catchment.

3.2 Bias correction

Rainfall downscaled from NCEP reanalysis and various GCM output datasets were bias corrected using the Frequency Adapted Quantile (FAQM) technique for the calibration (1961–1986), validation (1987–2000) and projection (2041–2060) periods. A detailed description of the FAQM bias-correction technique is found in the studies by Themeßl et al. (2012) and Rashid et al. (2015). In frequency adaptation, when the number of dry days of the downscaled rainfall is less than that of the observed rainfall, all the modelled rainfall that has a probability equal to or less than the probability of the observed zero rainfall is transferred to zero. On the other hand when the number of dry days of the downscaled rainfall is greater than that of the observed rainfall, a fraction of the simulated dry days is converted to wet days using randomly generated values following the gamma distribution of the downscaled rainfall. Once the frequency of the downscaled rainfall was corrected, quantile mapping (QM) was applied to correct the downscaled rainfall using a parameter free empirical distribution. In QM, the correction factor was estimated for each empirical cumulative distribution function (*ecdf*) of the downscaled rainfall by differencing the inverse cumulative distribution function (*ecdf*⁻¹) of downscaled and observed rainfall for the calibration period. Then the downscaled rainfall for the validation and future periods was corrected by

adding the correction factor to the uncorrected rainfall. If the downscaled rainfall in the validation or projection periods was outside the range of the rainfall in the calibration period, the new extreme rainfall values were corrected by constant extrapolation of the correction factor neglecting the four highest and lowest quantiles of the calibration period considering the assumption that the tail of the correction factor was likely to be noisy. The FAQM bias correction was applied to each downscaled rainfall series (downscaled from NCEP reanalysis and GCM datasets) considering the observed station rainfall as the base. In the case of downscaled rainfall from NCEP reanalysis datasets, correction factors for each quantile were estimated based on the observed rainfall for the calibration period. These correction factors were applied to correct rainfall for the calibration and validation periods. In the same way, correction factors were also estimated for the rainfall downscaled from GCM output datasets and used to correct rainfall for the historical (calibration and validation) and future projection periods.

3.3 Extreme rainfall indices

Extreme rainfall indices (listed in Table 2) were estimated from the observed and downscaled daily rainfall forced by NCEP reanalysis and GCM output datasets. The downscaling model performance was assessed for its ability to

Table 2 Extreme rainfall indices

Extreme rainfall indices	Description	Unit
RMD	Mean of daily rainfall on all days	mm/day
RDL90	Number of event > long-term 90th percentile rainfall	day
RQ90	Empirical 90th quantile of rainfall	mm
R5D	Maximum 5-day consecutive total rainfall	mm
CDD	Maximum number of consecutive dry days (daily rainfall < 1 mm)	day

reproduce the extreme rainfall indices for the calibration and validation periods in terms of the coefficient of determination (R^2), coefficient of efficiency (CE), mean bias (MB) and Nash-Sutcliffe efficiency (NS). Finally, the percentage change of the extreme rainfall indices was estimated for the future period (2041–2060) compared to the base period (1961–2000). The extreme rainfall indices considered in this study are listed in Table 2. These indices have also been used in different previous studies (Evans et al. 2009; Hashmi et al. 2011; Huang et al. 2012; Tryhorn and DeGaetano 2011; Yang et al. 2011).

3.4 Frequency analysis

Annual maximum daily rainfall (AMDR) series obtained from observed and downscaled daily rainfall (historical and projected) was used to estimate the 100-year AMDR. For this purpose, both stationary and non-stationary models were used. In the stationary model, the fitted distribution parameters are constant over the time. On the other hand, in the non-stationary model, the distribution parameters are considered as a function of certain explanatory variables so that parameters vary over time. GAMLSS (Rigby and Stasinopoulos 2005) has a flexible modelling framework which is suitable for non-stationary modelling of AMDR. In GAMLSS, the random response variable (AMDR for this study) has a parametric distribution function whose parameters can be modelled as a function of selected covariates (NCEP reanalysis and GCM output datasets in this study). Air temperature at 700 hPa; geopotential height at 700 and 800 hPa; relative humidity at 500, 700 and 850 hPa; zonal wind component at 700 and 850 hPa; and meridional wind component at 500 and 700 hPa were considered as the external covariates. The winter (June–August) means of these variables were extracted from the 12 grid points around the study area and spatially averaged which gives a single series for each variable used as a covariate for fitting a GAMLSS. The rationale of considering the winter average is that the most of the rainfall occurs over this period in this study area and in general the maximum correlation between observed AMDR and selected covariates occurred in winter.

A GAMLSS model assumes that for any observations for $i = 1, 2, 3, \dots, n$ independent observations, Y_i has a cumulative distribution function $F_{y_i}(Y_i|\theta_i)$, where $\theta_i = \theta_{i1}, \theta_{i2}, \theta_{i3}, \dots, \theta_{ip}$ is a vector of p distribution parameters accounting for location, scale and shape of the distribution. The number of parameters p generally varies from one to four. The model parameters are related to the covariates by a monotonic link function $g_k(\cdot)$ where $k = 1, 2, 3, \dots, p$ and the parameters are modelled through link functions. In this study, identity and logarithm link functions were considered. Details of GAMLSS are available in Stasinopoulos and Rigby (2007) and Rigby and Stasinopoulos (2005). While GAMLSS have several different

possible models, a semi-parametric additive model formulation was used in this study as follows:

$$g_k(\theta_k) = \eta_k = X_k \beta_k + \sum_{j=1}^{j_k} h_{jk}(x_{jk}) \quad (3)$$

where θ_k and η_k are vectors of length n , X_k is a matrix of covariates of order $n \times j_k$, $\beta_k = (\beta_{1k}, \dots, \beta_{j_k k})$ is a parameter vector of length j_k and $h_{jk}(\cdot)$ represents the dependence function of the distribution parameters on covariates. The dependence could be linear, or a smoothing term can be included to allow more flexibility for modelling the dependence of the distribution parameters on the covariates. Four distribution functions were considered in this study, namely the Gumbel, Lognormal, Weibull and Gamma distributions, as shown in Table 3. A stepwise model fitting approach proposed by Rigby and Stasinopoulos (2005) was followed to identify the significant covariates and distribution functions. In addition to the Akaike information criterion (AIC) and the Bayesian information criterion (BIC), model efficiency statistics such as the coefficient of determination (R^2), the root mean square error (RMSE) and the Nash-Sutcliffe (NS) efficiency were also assessed at each step of the model fitting. In addition, the normality and independence of the residuals were assessed by examining the first four moments of the residuals, by the Filliben correlation coefficient (Filliben 1975) and by visual inspection of a diagnostic plot of the residuals. Once the model was fitted, the distribution parameters were estimated for each data point and the 100-year AMDR were estimated based on the time-varying estimates of the model parameters θ_1 and θ_2 for the selected stations.

In order to assess the magnitude of the 100-year AMDR during the historical period (1961–2000) and the changes over the future period (2041–2060), four rainfall stations (G1, G3, G7 and G9) were considered for this study. These stations were selected to represent the upper, middle and downstream (near the coast) regions of the Onkapingara catchment (Fig. 1).

4 Results

4.1 Calibration and validation of the model

The model was able to reasonably reproduce the monthly statistics and variability of the extreme rainfall indices for both the calibration (1961–1986) and validation (1987–2000) periods. Figure 2 shows the observed and median simulated extreme rainfall indices for different months of the year for the validation period. Simulations were driven by the NCEP reanalysis and GCM historical datasets. In general, the simulation driven by the NCEP reanalysis datasets showed better agreement with the observed extreme rainfall indices than the simulation driven by GCM historical datasets. This is due to

Table 3 Probability density functions and their corresponding link functions

Distribution type	Probability distribution function	Link function $g(\cdot)$	
		θ_1	θ_2
Gumbel	$f_y(y \theta_1, \theta_2) = \frac{1}{\theta_2} \exp\left[\left(\frac{y-\theta_1}{\theta_2}\right) - \exp\left(\frac{y-\theta_1}{\theta_2}\right)\right]$ $-\infty < y < \infty, -\infty < \theta_1 < \infty, \theta_2 > 0$	Identity ()	$\ln ()$
Lognormal	$f_y(y \theta_1, \theta_2) = \frac{1}{\sqrt{2\pi\theta_2}} \frac{1}{y} \exp\left[-\frac{\{\log(y)-\theta_1\}^2}{2\theta_2^2}\right]$ $y > 0, \theta_1 > 0, \theta_2 > 0$	Identity ()	$\ln ()$
Weibull	$f_y(y \theta_1, \theta_2) = \frac{\theta_2 y^{\theta_2-1}}{\theta_1^{\theta_2}} \exp\left[-\left(\frac{y}{\theta_1}\right)^{\theta_2}\right]$ $y > 0, \theta_1 > 0, \theta_2 > 0$	$\ln ()$	$\ln ()$
Gamma	$f_y(y \theta_1, \theta_2) = \frac{1}{(\theta_2^2)^{\frac{1}{2}}} \frac{y^{\frac{1}{2}-1} \exp\left[\frac{-y}{\theta_2^2 \theta_1}\right]}{\Gamma\left(\frac{1}{\theta_2^2}\right)}$ $y > 0, \theta_1 > 0, \theta_2 > 0$	$\ln ()$	$\ln ()$

the bias between the NCEP reanalysis and GCM datasets. The FAQM correction technique that was applied significantly reduced the bias in extreme rainfall indices. However, the maximum 5-day rainfall total was still underestimated by all simulations during the months from June to October. This might be due to an underestimation of rainfall amounts and consecutive wet days during this period of the year. The maximum consecutive dry days (CDD) was also underestimated for the months January to May for all simulations.

Table 4 shows the performance after bias correction of the statistical downscaling model driven by NCEP reanalysis data and different GCMs in terms of the coefficient of determination (R^2), coefficient of efficiency (CE), mean bias (MB) and Nash-Sutcliffe efficiency (NS) for the validation period. The efficiency statistics were found to be reasonable for all models, and in general, the model driven by NCEP reanalysis data showed better performance than the model driven by GCM historical outputs. The values shown in italic text in Table 4 are the NS statistics before bias correction. The results show that the FAQM technique was able to reasonably correct the bias for extreme rainfall indices such as RDM, RDL90, RQ90 and R5D. However, in contrast, the model efficiency for CDD deteriorated after bias correction. For the FAQM bias correction technique, when the number of dry days of the downscaled rainfall was greater than that of the observed rainfall, a certain fraction of the simulated dry days was converted to wet days by randomly replacing the values obtained from randomly generated values following the gamma distribution of the modelled rainfall. This is likely to break the long dry spells which eventually reduces the maximum consecutive dry days (CDD).

Moreover, quantile mapping (QM) can correct the bias in rainfall quantity but it cannot correct the sequence of dry and wet days. While uncorrected downscaled daily rainfall showed a good degree of efficiency in terms of reproducing CDD statistics, as listed in Table 4, downscaled daily rainfall series without correction were used instead to estimate the future changes of CDD. However, it is expected that developing a bias correction technique based on the transitional probability of dry and/or wet days and applying this technique to simulated CDD series would reduce the bias in CDD.

4.2 Future changes in extreme rainfall indices

Changes in the extreme rainfall indices for different GCMs under RCP4.5 and RCP8.5 scenarios over the period 2041–2060 compared to the base period 1961–2000 are shown in Fig. 3 (RDM, RDL90 and RQ90) and Fig. 4 (R5D and CDD). Future projected changes are shown for each month of the year. Although a few model-month combinations showed that RDM, RDL90 and R5D would increase and CDD would decrease, most of the model-month combinations showed that RDM, RDL90, RQ90 and R5D would decrease whereas CDD would increase for both the RCP4.5 and RCP8.5 scenarios. Future changes of RDM, RDL90, RQ90, R5D and CDD range from 12.65 to -40.19% , 23.27 to -50% , 11.25 to -47.53% , 21.76 to -37.26% and 34.68 to -12.96% , respectively, for the RCP4.5 scenario and 16.9 to -45.66% , 22.12 to 67.3%, 19.16 to 51.69%, 22.81 to -40.32% and 30.23 to -7.31% , respectively, for the RCP8.5 scenario. The highest reduction in extreme indices is seen to occur during September to January

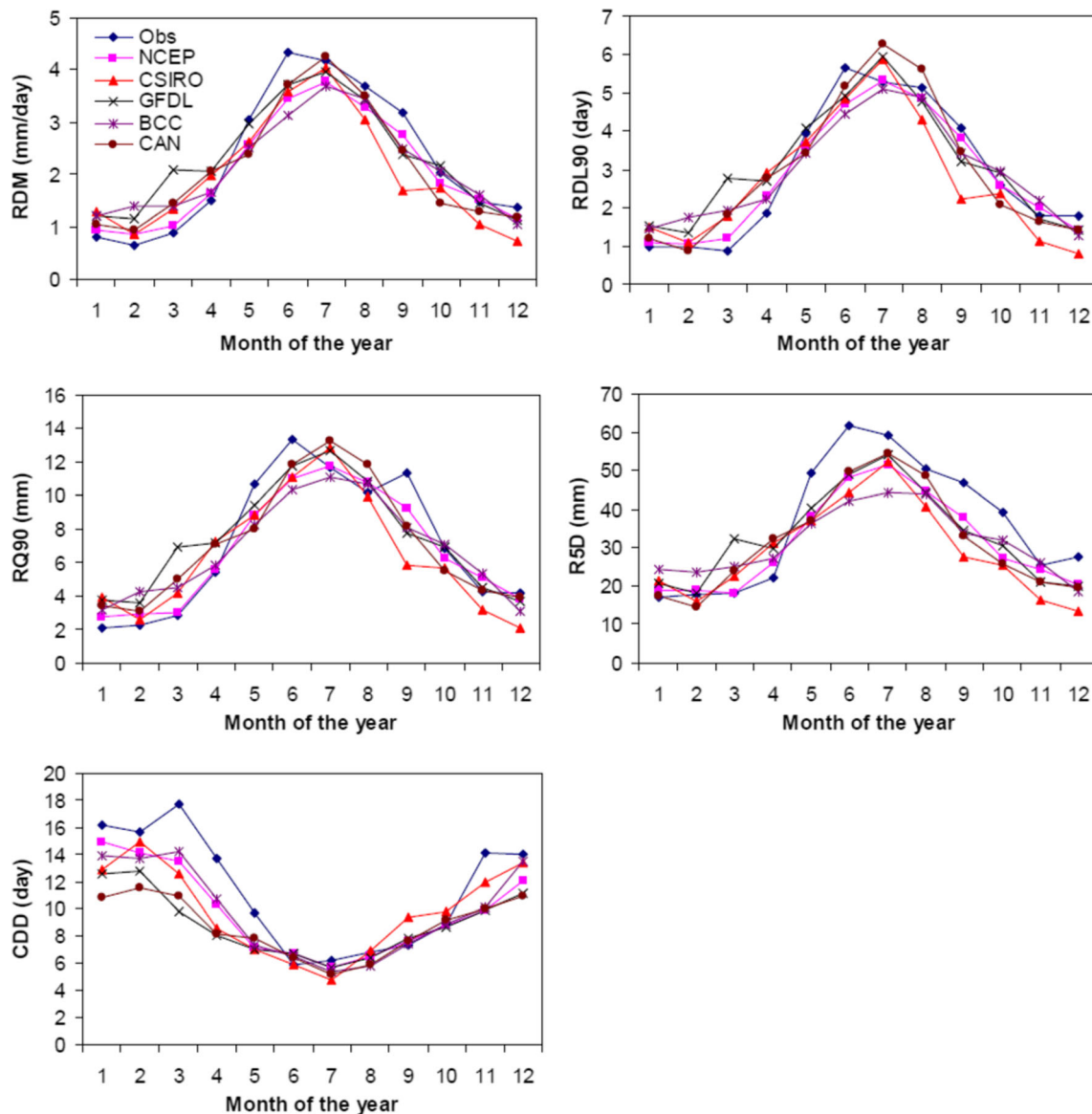


Fig. 2 Comparison of extreme rainfall indices from observed and median simulated rainfall driven by NCEP reanalysis and GCM historical datasets for the validation period (1987 to 2000)

whereas the lowest reduction occurs during the period May to August. This tendency is more prominent under the RCP8.5 than RCP4.5 scenario. This reveals that there is a possibility of higher reductions in rainfall amount-related indices (RDM, RDL90, RQ90 and R5D) in the dry season compared to the wet season, which indicates that a regional drought will be intensified in the future (2041–2060) compared to the historical period (1961–2000). Rashid et al. (2015) also observed significant reductions in annual and seasonal rainfall for the future period 2041–2060 in the Onkapinga catchment.

An increase in the maximum number of consecutive dry days (CDD) may also intensify the droughts that are periodically experienced in the Onkapinga catchment. These changes of daily rainfall occurrence sequences and reduction in the rainfall amount will reduce the runoff potential, which will eventually

affect regional water availability. Obviously, the magnitude of changes in the extreme rainfall indices varies with the models and scenarios due to differences in the model settings and scenarios. However, in general, the direction of changes was found to be consistent for all models and scenarios.

4.3 AMDR

The downscaling model was able to reasonably reproduce the AMDR when forced by NCEP reanalysis and GCM historical datasets. Figure 5 shows a comparison between the observed and simulated AMDR when forced by NCEP reanalysis datasets at nine rainfall stations for the calibration (1961–1986) and validation (1987–2000) periods. The 2.5th and 97.5th percentiles of the AMDR series were generated from

Table 4 Downscaling model efficiency for the validation period after bias correction

Indices	Model	R ²	CE	MB	NS
RDM	NCEP	0.98	0.74	-0.20	0.91 (0.87)
	CSIRO	0.81	0.55	-0.27	0.76 (0.71)
	GFDL	0.87	0.64	0.05	0.83 (0.65)
	BCC	0.91	0.62	-0.13	0.82 (0.64)
	CAN	0.89	0.65	-0.12	0.87 (0.66)
RDL90	NCEP	0.97	0.82	-0.08	0.95 (0.87)
	CSIRO	0.77	0.54	-0.20	0.8 (0.75)
	GFDL	0.82	0.62	0.21	0.81 (0.72)
	BCC	0.91	0.65	0.01	0.87 (0.69)
	CAN	0.89	0.67	0.07	0.88 (0.72)
RQ90	NCEP	0.94	0.76	-0.32	0.91 (0.85)
	CSIRO	0.72	0.52	-0.62	0.74 (0.70)
	GFDL	0.79	0.59	0.33	0.77 (0.67)
	BCC	0.86	0.60	-0.26	0.80 (0.65)
	CAN	0.80	0.58	0.05	0.80 (0.63)
R5D	NCEP	0.93	0.58	-5.02	0.80 (0.78)
	CSIRO	0.71	0.32	-7.21	0.73 (0.50)
	GFDL	0.79	0.49	-3.35	0.71 (0.51)
	BCC	0.83	0.39	-4.81	0.59 (0.38)
	CAN	0.80	0.49	-4.80	0.70 (0.53)
CDD	NCEP	0.88	0.54	-1.59	0.69 (0.88)
	CSIRO	0.73	0.48	-1.52	0.59 (0.59)
	GFDL	0.70	0.30	-2.48	0.26 (0.73)
	BCC	0.91	0.57	-1.57	0.74 (0.89)
	CAN	0.81	0.27	-2.64	0.25 (0.77)

Italic text in brackets represents the NS statistics before bias correction
*R*² coefficient of determination, *CE* coefficient of efficiency, *MB* mean bias, *NS* Nash-Sutcliffe efficiency

1000 sets of simulations and are presented as dotted lines. The thick black line represents the median simulated AMDR. For most of the year, the AMDR were within the simulation envelop for all stations. Similar model efficiency was also observed for the simulations driven by the GCM historical datasets including CSIRO, GFDL, BCC and CAN after bias correction. However, the model was limited in its ability to reproduce the inter-annual variability of the AMDR for all simulations forced by the NCEP reanalysis and GCM historical datasets at all stations. AMDR is the maximum daily rainfall value over a year. For a daily rainfall model, it is difficult to accurately reproduce such extreme values for each year over the modelling period. Moreover, the gamma distribution used in the downscaling model has limited ability to capture the extreme rainfall (Rashid et al. 2014). In addition, downscaling of AMDR is challenging due to its high spatial and temporal variability and non-linear nature. Direct downscaling of AMDR from reanalysis and GCM output datasets by considering AMDR as a predictand might resolve this problem.

4.4 Frequency analysis of AMDR

Figure 6 shows the results of the non-stationary modelling of the observed rainfall and 100-year AMDR magnitude for the representative sites. The non-stationary model was developed by fitting a GAMLSS to the observed AMDR considering the NCEP reanalysis variables as external covariates. In the same way for the median simulated AMDR driven by different GCMs, historical and projected (RCP4.5 and RCP8.5) GCM output datasets were considered as external covariates. Several of the selected external covariates were found to vary between the rainfall stations. It was found that the gamma (for station G1) and lognormal distributions (for stations G3, G7 and G9) gave the best overall results for the observed AMDR. The non-linear dependence of external covariates using cubic splines was found to be significant for the distribution parameter θ_1 for all stations. To reduce overfitting of the model, the distribution parameter θ_2 was considered constant. The model efficiency statistics such as the coefficient of determination (*R*²), root mean square error (RMSE) and Nash-Sutcliffe (NS) were found to be reasonable for each station. Figure 6 shows the magnitude of the 100-year AMDR under both stationary and non-stationary conditions. In the non-stationary frequency analysis, the distribution parameters were considered to be varied over time whereas in the stationary modelling they were considered constant. It was observed that the non-stationary model showed significant variability in the AMDR frequency. The results show that the stationary model could lead to significant underestimation or overestimation of the rainfall compared to the non-stationary model. For example, at site G9, the non-stationary frequency analysis indicated that the 100-year AMDR during the 40 years (1961–2000) of the observation period varied from a maximum of 142 mm/day in 1969 to a minimum of 28.5 mm/day as shown in Fig. 6, whereas the 100-year AMDR was 83.52 mm/day for the stationary frequency analysis. Similar results were also observed for other stations.

The non-stationary frequency analysis of AMDR obtained from the downscaled simulations driven by different GCM datasets shows that the 100-year AMDR (annual exceedance probability of 0.01) varies significantly (decreases and increases) over the periods 1960–2000 and 2041–2060. So in the non-stationary frequency analysis, the 100-year AMDR includes maximum and minimum values over a historical or future period. Table 5 lists the change in the maximum and minimum values of the 100-year AMDR for the future period (2041–2060) compared to the base period (1961–2000). It was observed that the degree of change varies with the selected models and scenarios. In general, maximum and minimum values of the 100-year AMDR are likely to decrease over the period 2041–2060 for all models and scenarios. An exception was observed for the downscaled simulation forced by the CSIRO GCM, which showed that the maximum of the 100-year AMDR would increase during the period 2041–2060 for the RCP8.5 scenario.

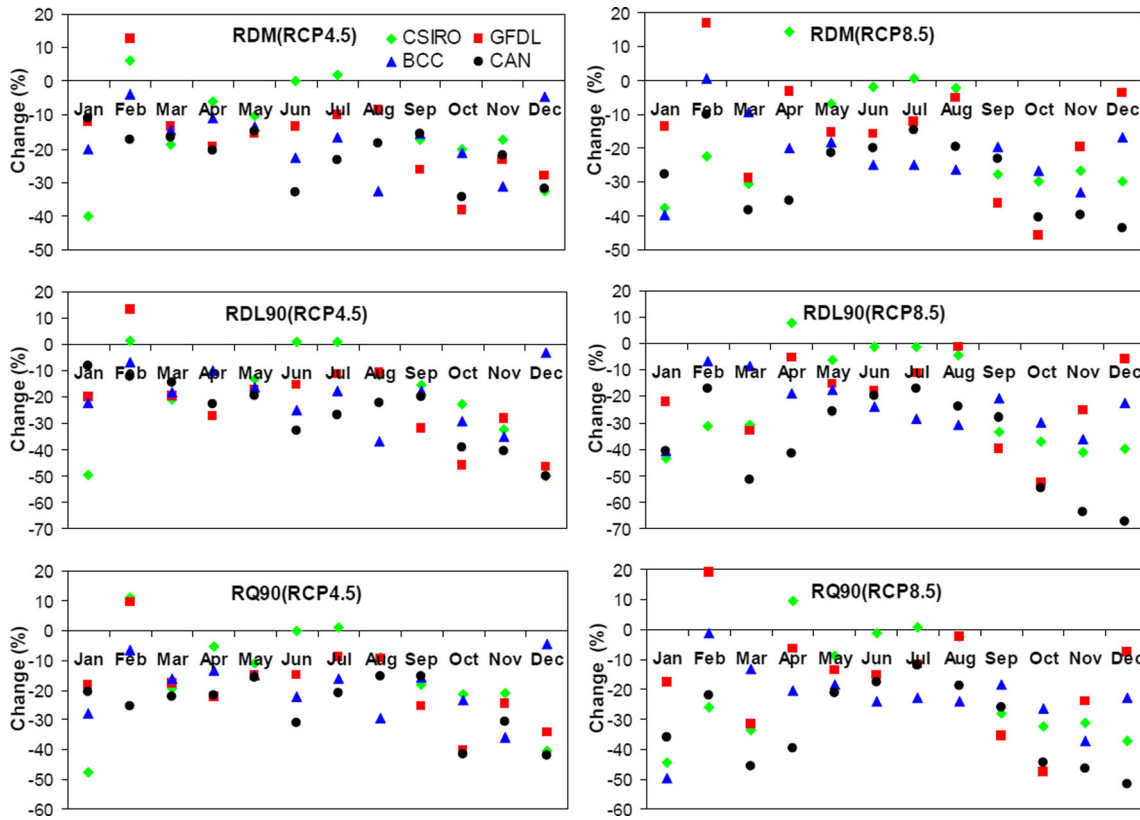


Fig. 3 Changes in extreme rainfall indices (RDM, RDL90 and RQ90) for different GCMs under scenarios RCP4.5 (left column) and RCP8.5 (right column) for the future period (2041 to 2060) compared to the base period (1961 to 2000)

5 Discussion

Even though the magnitude of changes in extreme rainfall varies for the future period, the direction of changes is consistent for all CMIP GCM models and scenarios. This gives some confidence in the projected changes presented in this study, although uncertainties still need to be considered. The future changes of extreme

rainfall indices and annual maximum daily rainfall projected in this study may not account for the full range of climate change impacts because these are based on a small number of GCMs and scenarios due to data availability. Nevertheless, the methodology developed in this study can be applied to assess the future changes of extreme rainfall for other GCM scenarios through downscaling rainfall from those GCMs and scenarios.

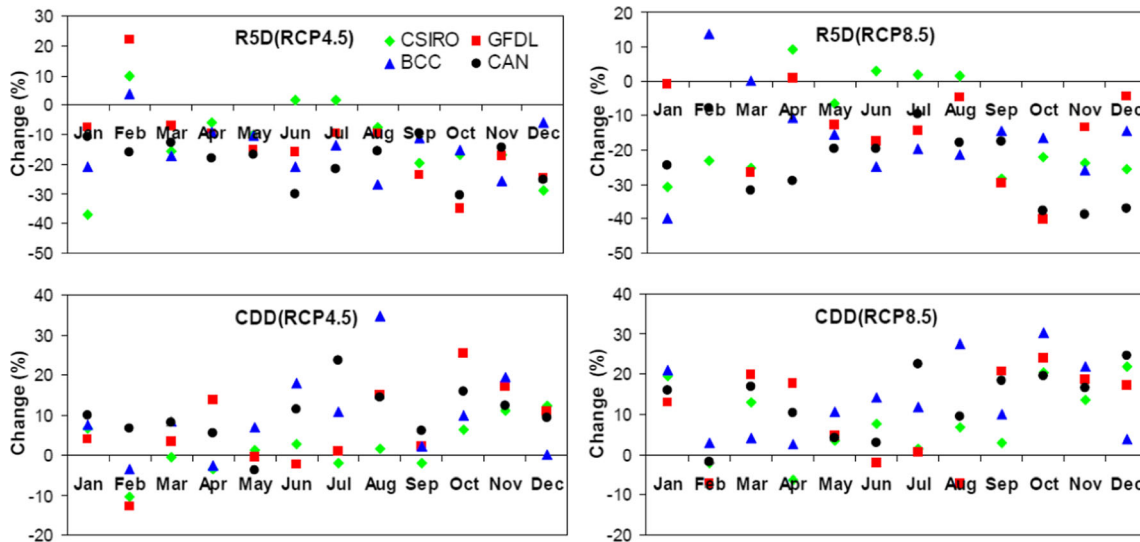


Fig. 4 Same as Fig. 2 but for R5D and CDD

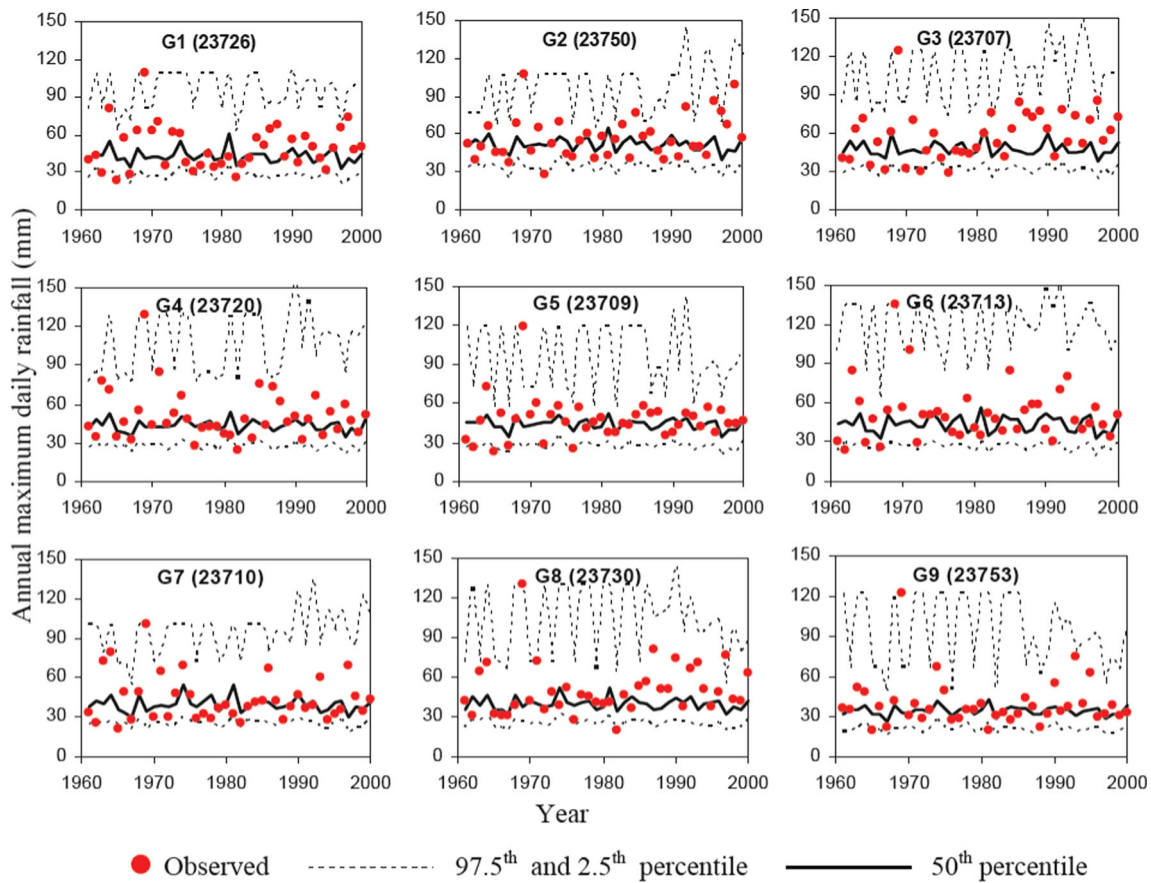


Fig. 5 Observed and NCEP simulated annual maximum daily rainfall at different rainfall stations for the calibration (1961 to 1986) and validation (1987 to 2000) periods

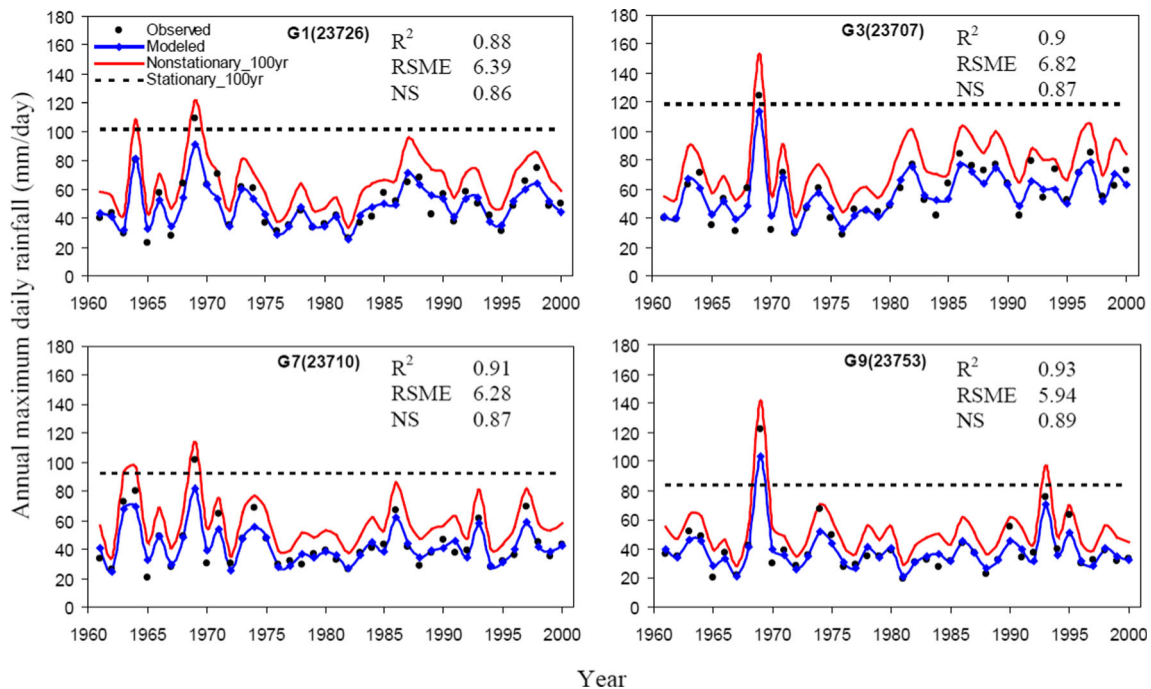


Fig. 6 Non-stationary modelled AMDR (blue line) and quantile estimates of AMDR with 0.01 annual exceedance probability for the period 1961 to 2000 based on stationary (dotted black line) and non-stationary (red line) models. The small black circles represent the observed AMDR

Table 5 Change in maximum and minimum values of 100-year AMDR for different GCMs and scenarios for the future period (2041–2060) compared to the base period (1960–2000)

Station	GCM	Maximum 100-year AMDR		Minimum 100-year AMDR	
		RCP4.5	RCP8.5	RCP4.5	RCP8.5
G1	CSIRO	-7 %↓	+5 %↑	-3 %↓	-8 %↓
	GFDL	-21 %↓	-12 %↓	-16 %↓	-15 %↓
	BCC	-24 %↓	-25 %↓	-18 %↓	-20 %↓
	CAN	-35 %↓	-26 %↓	-16 %↓	-11 %↓
G3	CSIRO	-6 %↓	+16 %↑	-6 %↓	-5 %↓
	GFDL	-13 %↓	-9 %↓	-17 %↓	-11 %↓
	BCC	-19 %↓	-18 %↓	-15 %↓	-15 %↓
	CAN	-29 %↓	-28 %↓	-11 %↓	-10 %↓
G7	CSIRO	-1 %↓	+29 %↑	-7 %↓	-3 %↓
	GFDL	+1 %↑	-5 %↓	-19 %↓	-18 %↓
	BCC	-22 %↓	-22 %↓	-18 %↓	-23 %↓
	CAN	-42 %↓	-34 %↓	-14 %↓	-10 %↓
G9	CSIRO	-1 %↓	+14 %↑	-13 %↓	-6 %↓
	GFDL	-3 %↓	0 % =	-21 %↓	-20 %↓
	BCC	-14 %↓	-18 %↓	-20 %↓	-21 %↓
	CAN	-27 %↓	-28 %↓	-6 %↓	-7 %↓

Extreme climate conditions depend on large-scale processes that modify the stability of the atmosphere by exchanging mass and energy from the oceans to the atmosphere and from the equator to the poles. The specific influence of large-scale processes on South Australian extreme rainfall is not well understood. Evans et al. (2009) concluded that extreme rainfall over SA is linked to the large-scale rearrangement of circulation patterns. Their study reveals that meridional sea surface temperature (SST) in the eastern Indian Ocean (EIO) influences extreme rainfall events over SA. During dry winters, pole-ward shifts of the westerlies to the south of Australia and increased offshore flow over the northwest of Australia reduce advection of moist warm air into SA from the northwest and moist cold air along the southern coastline. Thus, the interaction of these air masses is reduced which eventually decreases rainfall in SA (Evans et al. 2009). In addition to large-scale processes, mesoscale weather system is also responsible to modulate the local-scale extreme rainfall. So, extreme rainfall is location specific. While extreme rainfall is likely to increase over the southern and southwestern flatlands (east) of Australia (CSIRO and BOM 2015; IPCC 2012), our study shows that amount-related extreme rainfall indices and AMDR are likely to decrease in future over the Onkaparinga catchment. It should be noted that the GCMs are unable to capture the mesoscale atmospheric features such as geography that modifies the atmospheric flow, small horizontal shifts in storm movement, land use changes and clouds

which essentially influence the local-scale extreme rainfall (Tisseuil et al. 2010; Willems et al. 2012). Moreover, rainfall events averaged over a large spatial scale are not able to represent the extreme rainfall events that occur at a far smaller spatial scale. This reveals the necessity of catchment scale assessment of extreme rainfall in a changed climate.

In addition to natural variations in the climatic system, anthropogenic-induced climate change due to greenhouse gas emissions changes the hydrological cycle creating a situation whereby stationarity in hydro-climatic variables such as rainfall is no longer valid. This study has shown that using large-scale climatic variables as covariates in a non-stationary model of AMDR can produce reliable scenarios of future extreme rainfall.

6 Conclusion

In this study, the performance of the GLIMCLIM statistical downscaling model was first assessed in terms of its ability to simulate extreme rainfall indices and annual maximum daily rainfall (AMDR) when daily rainfall was downscaled from NCEP reanalysis and CMIP5 GCM output datasets. Then the changes in extreme rainfall indices and 100-year AMDR were estimated using four different CMIP5 GCMs (CSIRO, GFDL, BCC and CAN) under RCP4.5 and RCP8.5 scenarios for the future period of 2041–2060 compared to the base period of 1961–2000. The downscaling model was able to reasonably reproduce the monthly statistics and variability of the extreme rainfall indices for both the calibration (1961–1986) and validation (1987–2000) periods when driven by the NCEP reanalysis datasets. However, the model showed less skill in reproducing the extreme rainfall indices when forced by the CMIP5 GCM historical output datasets.

Frequency Adapted Quantile Mapping was applied to the simulated daily rainfall series, and this significantly reduced the bias in the extreme rainfall indices. However, the model efficiency for consecutive dry days (CDD) deteriorated after bias correction. This might be due to the fact that during the frequency adaptation, imputation of random values to turn the dry days to wet days might break the dry spell and reduce the maximum consecutive dry days. The downscaling model was found to be able to reasonably reproduce the AMDR for both the calibration and validation periods. For almost all years, the observed AMDR were within the 2.5th and 97.5th percentiles of the simulated rainfall. However, inter-annual variability of AMDR was underestimated in all models.

This study has shown that extreme indices related to rainfall amount are likely to decrease for all models and scenarios. This reduction will be higher during the dry season compared to the wet season, which points toward a regional water scarcity situation in the future (2041–2060), when the dry season will be drier compared to the present time (1961–2000). In

addition, the maximum number of consecutive dry days (CDD) will increase in future and this will intensify future droughts in the Onkaparinga catchment.

It was also found in this study that the GAMLSS provides a flexible modelling framework for representing the non-stationary behaviour of AMDR. In particular, the gamma and lognormal distributions gave the best fit for AMDR. Non-linear dependence of external covariates (NCEP reanalysis and CMIP5 GCM output datasets) was found to be significant for selected distribution parameters. In general, future projections show that both the minimum and maximum values of the 100-year AMDR are likely to decrease over the future period (2041–2060) compared to the base period (1961–2000) for all models and scenarios at all selected rainfall stations. However, an exception was observed for the CSIRO GCM, which projected that the maximum 100-year AMDR will increase for all selected sites under the RCP8.5 scenario.

Overall, the downscaling model was able to reasonably simulate the extreme rainfall indices and AMDR in the Onkaparinga catchment. Generally, the direction of changes was consistent for all models and scenarios. This indicates that the Onkaparinga catchment will experience drier conditions due to an increase in consecutive dry days coinciding with decreases in heavy rainfall days, empirical 90th quantile of rainfall and maximum 5-day consecutive total rainfall for the future period (2041–2060) compared to the base period (1961–2000).

References

- Aissaoui-Fqayeh I, El-Adlouni S, Ouarda T, St-Hilaire A (2009) Non-stationary lognormal model development and comparison with non-stationary GEV model. *Hydrol Sci J* 54:1141–1156
- Alexander LV, Arblaster JM (2009) Assessing trends in observed and modelled climate extremes over Australia in relation to future projections. *Int J Climatol* 29:417–435
- Alexander L, Zhang X, Peterson T, Caesar J, Gleason B, Klein Tank A, Haylock M, Collins D, Trewin B, Rahimzadeh F (2006) Global observed changes in daily climate extremes of temperature and precipitation. *J Geophys Res Atmos* (1984–2012):111
- Alexander LV, Hope P, Collins D, Trewin B, Lynch A, Nicholls N (2007) Trends in Australia's climate means and extremes: a global context. *Aust Meteorol Mag* 56:1–18
- Beecham S, Rashid M, Chowdhury RK (2014) Statistical downscaling of multi-site daily rainfall in a South Australian catchment using a Generalized Linear Model. *Int J Climatol R Meteorol Soc* 34. doi:10.1002/joc.3933
- Chandler RE (2002) GLIMCLIM: generalised linear modelling for daily climate time series (software and user guide)
- Chandler RE, Wheeler HS (2002) Analysis of rainfall variability using generalized linear models: a case study from the west of Ireland. *Water Resour Res* 38:1–11. doi:10.1029/2001wr000906
- Chu J, Xia J, Xu C-Y, Singh V (2010) Statistical downscaling of daily mean temperature, pan evaporation and precipitation for climate change scenarios in Haihe River, China. *Theor Appl Climatol* 99:149–161
- Collins D, Della-Marta P, Plummer N, Trewin B (2000) Trends in annual frequencies of extreme temperature events in Australia. *Aust Meteorol Mag* 49:277–292
- CSIRO BOM (2015) Climate change in Australia information for Australia's natural resource management regions: technical report. CSIRO and Bureau of Meteorology, Australia
- El Adlouni S, Ouarda T, Zhang X, Roy R, Bobée B (2007) Generalized maximum likelihood estimators for the nonstationary generalized extreme value model. *Water Resour Res* 43:W03410. doi:10.1029/2005WR004545
- Evans AD, Bennett JM, Ewenz CM (2009) South Australian rainfall variability and climate extremes. *Clim Dyn* 33:477–493. doi:10.1007/s00382-008-0461-z
- Filliben JJ (1975) The probability plot correlation coefficient test for normality. *Technometrics* 17:111–117
- Frei C, Schöll R, Fukutome S, Schmidli J, Vidale PL (2006) Future change of precipitation extremes in Europe: intercomparison of scenarios from regional climate models. *J Geophys Res Atmos* (1984–2012):111
- Frich P, Alexander L, Della-Marta P, Gleason B, Haylock M, Klein Tank A, Peterson T (2002) Observed coherent changes in climatic extremes during the second half of the twentieth century. *Clim Res* 19:193–212
- Frost AJ (2007) Australian application of a statistical downscaling technique for multi-site daily rainfall: GLIMCLIM. *Model Simul Soc Aust N Z* 553–559
- Frost AJ, Charles SP, Timbal B, Chiew FHS, Mehrotra R, Nguyen KC, Chandler RE, McGregor JL, Fu G, Kirono DGC, Fernandez E, Kent DM (2011) A comparison of multi-site daily rainfall downscaling techniques under Australian conditions. *J Hydrol* 408:1–18. doi:10.1016/j.jhydrol.2011.06.021
- Hashmi MZ, Shamseldin AY, Melville BW (2011) Comparison of SDSM and LARS-WG for simulation and downscaling of extreme precipitation events in a watershed. *Stoch Env Res Risk A* 25:475–484
- Haylock M, Nicholls N (2000) Trends in extreme rainfall indices for an updated high quality data set for Australia, 1910–1998. *Int J Climatol* 20:1533–1541
- Heneker TM, Cresswell D (2010) Potential impact on water resource availability in the Mount Lofty Ranges due to climate change. Technical report DFW 2010/03. Department for Water, Government of South Australia
- Hennessy KJ, Suppiah A, Forland E, Zhai P (1999) Australian rainfall changes, 1910–1995. *Australian Meteorology Magazine* 48:1–13
- Hu Y, Maskey S, Uhlenbrook S (2012) Downscaling daily precipitation over the Yellow River source region in China: a comparison of three statistical downscaling methods. *Theor Appl Climatol* 112:447–460. doi:10.1007/s00704-012-0745-4
- Hu Y, Maskey S, Uhlenbrook S (2013) Downscaling daily precipitation over the Yellow River source region in China: a comparison of three statistical downscaling methods. *Theor Appl Climatol* 112:447–460
- Huang J, Zhang J, Zhang Z, Xu CY, Wang B, Yao J (2011) Estimation of future precipitation change in the Yangtze River basin by using statistical downscaling method. *Stoch Env Res Risk A* 25:781–792
- Huang J, Zhang J, Zhang Z, Sun S, Yao J (2012) Simulation of extreme precipitation indices in the Yangtze River basin by using statistical downscaling method (SDSM). *Theor Appl Climatol* 108:325–343. doi:10.1007/s00704-011-0536-3
- Hundecha Y, Bárdossy A (2008) Statistical downscaling of extremes of daily precipitation and temperature and construction of their future scenarios. *Int J Climatol* 28:589–610
- IPCC (2007) Change 2007: the physical science basis. Contribution of Working Group I to the Fourth Assessment Report of the Intergovernmental Panel on Climate Change. Cambridge University Press, Cambridge, UK and New York, NY USA

- IPCC (2012) Managing the risks of extreme events and disasters to advance climate change adaptation. A special report of Working Groups I and II of the Intergovernmental Panel on Climate Change. Cambridge University Press, Cambridge, UK, and New York, NY, USA
- Jeong DI, St-Hilaire A, Ouarda TBMJ, Gachon P (2012) Projection of future daily precipitation series and extreme events by using a multi-site statistical downscaling model over Montréal, Québec, Canada. *Hydrol Res* 44(1):147–168. doi:10.2166/nh.2012.183
- Kharin VV, Zwiers FW, Zhang X, Hegerl GC (2007) Changes in temperature and precipitation extremes in the IPCC ensemble of global coupled model simulations. *J Clim* 20:1419–1444
- Kigobe M, McIntyre N, Wheeler H, Chandler R (2011) Multi-site stochastic modelling of daily rainfall in Uganda. *Hydrol Sci J* 56:17–33
- King LM, Irwin S, Sarwar R, McLeod AIA, Simonovic SP (2012) The effects of climate change on extreme precipitation events in the upper Thames River basin: a comparison of downscaling approaches. *Canadian Water Resources Journal* 37:253–274
- Klein Tank AMG, Zwiers FW, Zhang X (2009) Guidelines on analysis of extremes in a changing climate in support of informed decisions for adaptation. Climate data and monitoring WCDMP No72, WMO-TD No 1500, 56 pp
- Kwon HH, Brown C, Lall U (2008) Climate informed flood frequency analysis and prediction in Montana using hierarchical Bayesian modeling. *Geophys Res Lett* 35:L05404. doi:10.1029/2007GL032220
- Li Y, Cai W, Campbell E (2005) Statistical modeling of extreme rainfall in southwest Western Australia. *J Clim* 18:852–863
- Liu W, Fu G, Liu C, Charles SP (2012) A comparison of three multi-site statistical downscaling models for daily rainfall in the North China Plain. *Theor Appl Climatol*. doi:10.1007/s00704-012-0692-0
- López J, Francés F (2013) Non-stationary flood frequency analysis in continental Spanish rivers, using climate and reservoir indices as external covariates. *Hydrol Earth Syst Sci* 17:3189–3203
- Mehrotra R, Sharma A, Srikanthan S, Frost AJ (2009) Comparison of statistical downscaling techniques for multisite daily rainfall conditioned on atmospheric variables for the Sydney region. *Australian Journal of Water Resources* 13:1–15
- Mirshahi B, Onof C, Wheeler HS (2008) Spatialtemporal daily rainfall simulation for a semi-arid area in Iran: a preliminary evaluation of generalised linear models. Sustainable Hydrology for the 21st Century, Proceedings of the 10th BHS National Hydrology Symposium, 2008, 145–152
- Ouarda T, El-Adlouni S (2011) Bayesian nonstationary frequency analysis of hydrological variables 1. Wiley Online Library
- Plummer N, Salinger MJ, Nicholls N, Suppiah R, Hennessy KJ, Leighton RM, Trewin B, Lough JM (1999) Twentieth century trends in climate extremes over the Australian region and New Zealand. *Climate Change* 42:183–202
- Rashid MM, Beecham S, Chowdhury RK (2014) Statistical characteristics of rainfall in the Onkaparinga catchment in South Australia. *Journal of Water and Climate Change*, IWA Publishing 6:352–372. doi:10.2166/wcc.2014.031
- Rashid M, Beecham S, Chowdhury RK (2015) Statistical downscaling of CMIP5 outputs to rainfall and projections of future changes. *Science of the Total Environment*, Elsevier 530:171–182. doi:10.1016/j.scitotenv.2015.05.024
- Rigby R, Stasinopoulos D (2005) Generalized additive models for location, scale and shape. *J R Stat Soc: Ser C: Appl Stat* 54:507–554
- Sachindra D, Huang F, Barton A, Perera B (2014) Statistical downscaling of general circulation model outputs to precipitation—part 2: bias-correction and future projections. *Int J Climatol* 34:3282–3303. doi:10.1002/joc.3915
- Sillmann J, Kharin V, Zhang X, Zwiers F, Bronaugh D (2013) Climate extremes indices in the CMIP5 multimodel ensemble: part 1. Model evaluation in the present climate. *Journal of Geophysical Research: Atmospheres* 118:1716–1733
- Stasinopoulos DM, Rigby RA (2007) Generalized additive models for location scale and shape (GAMLSS) in R. *J Stat Softw* 23:1–46
- Suppiah R, Hennessy KJ (1998) Trend in total rainfall, heavy-rain events and number of dry days in Australia, 1910–1990. *Int J Climatol* 10:1141–1164
- Tebaldi C, Hayhoe K, Arblaster JM, Meehl GA (2006) Going to the extremes: an intercomparison of model-simulated historical and future changes in extreme events. *Clim Chang* 79:185–211. doi:10.1007/s10584-006-9051-4
- Teng J, Chiew FH, Vaze J (2012) Will CMIP5 GCMs reduce or increase uncertainty in future runoff projections. American Geophysical Union—Fall Meeting, 3–7 December 2012, San Francisco, USA
- Teoh KS (2003) Estimating the impact of current farm dams development on the surface water resources of the Onkaparinga River Catchment. DWLBC Report 2002/22, Department of Water, Land and Biodiversity Conservation, for the Government of South Australia
- Themeßl MJ, Gobet A, Heinrich G (2012) Empirical-statistical downscaling and error correction of regional climate models and its impact on the climate change signal. *Clim Chang* 112:449–468
- Tisseuil C, Vrac M, Lek S, Wade AJ (2010) Statistical downscaling of river flows. *J Hydrol* 385:279–291
- Tramblay Y, Neppel L, Carreau J, Najib K (2013) Non-stationary frequency analysis of heavy rainfall events in southern France. *Hydrol Sci J* 58:280–294
- Tryhorn L, DeGaetano A (2011) A comparison of techniques for downscaling extreme precipitation over the northeastern United States. *Int J Climatol* 31:1975–1989
- Villarini G, Smith JA, Serinaldi F, Bales J, Bates PD, Krajewski WF (2009) Flood frequency analysis for nonstationary annual peak records in an urban drainage basin. *Adv Water Resour* 32:1255–1266
- Wang B, Yim S-Y, Lee J-Y, Liu J, Ha K-J (2014) Future change of Asian-Australian monsoon under RCP 4.5 anthropogenic warming scenario. *Clim Dyn* 42:83–100
- Willems P, Olsson J, Arnbjerg-Nielsen K, Beecham S, Pathirana A, Gregersen IB, Madsen H, Nguyen VTV (2012) Impacts of climate change on rainfall extremes and urban drainage systems. IWA Publishing
- Yang C, Chandler RE, Isham VS, Wheeler HS (2005) Spatial-temporal rainfall simulation using generalized linear models. *Water Resource Research* 41:1–13. doi:10.1029/2004wr003739
- Yang T, Li H, Wang W, Xu CY, Yu Z (2011) Statistical downscaling of extreme daily precipitation, evaporation, and temperature and construction of future scenarios. *Hydrol Process* 26:3510–3523